

# Expansion of Laser-Generated Plumes Near the Plasma Ignition Threshold

Laszlo Balazs

Central Research Institute for Physics of the Hungarian Academy of Sciences, P.O. Box 49, H-1525 Budapest 114, Hungary

Renaat Gijbels and Akos Vertes\*

University of Antwerp (U.I.A.), Department of Chemistry, Universiteitsplein 1, B-2610 Wilrijk, Belgium

**Expansion of laser-produced plumes on a solid-vacuum interface during and after the laser shot was investigated theoretically, incorporating several new features into our previous one-component one-dimensional hydrodynamic model. Time development of density, velocity, temperature, and pressure profiles was calculated at laser irradiances below and above the plasma ignition threshold. The estimated velocity of ions released from the plume was close to the measured values. The fast spreading of the blow-off material under the laser vaporization regime and the long lifetime of the relatively compact plasma core above the ignition threshold were predicted in agreement with experimental observations. Calculated surface recession due to evaporation provided a lower bound to the measured crater depth, whereas the calculated melt depth proved to be a realistic upper limit.**

## INTRODUCTION

When a high-power laser pulse is focused onto a solid surface, the irradiance in the focal spot can lead to rapid local heating, intense evaporation, and degradation of the material.

In analytical chemistry several exploited and potential uses of such processes exist. Most eminent among them is its application in mass spectrometry as an ion source in a vacuum environment (1-3). Further possibilities lie with the utilization as an optical emission source (4) or as a universal tool for sampling solids (5-8). Laser desorption and volatilization found their way to applications in interfacing thin-layer chromatography to gas chromatography (9) and to mass spectrometry (10).

The most attractive features of laser excitation are its capability to probe insulators—an area where most other methods encounter difficulties—and its cleanliness in depositing energy; i.e. no contamination from electrodes or plasma supporting gases can occur. Furthermore, short laser pulses (ranging routinely from picoseconds to nanoseconds)

often offer advantages in analysis, like for example the application of time of flight ion analyzers. Easy tuning of the delivered energy amount and the possibility of localized sampling supplement the list of benefits.

The difficulty related to laser excitation is that the sample has to absorb the light at the particular wavelength, a prerequisite often met in the ultraviolet region. Further problems are the high cost and complexity of the laser systems and the poor understanding of laser-induced processes. Both of these shortcomings are likely to improve in the near future. In this paper we will try to unveil some of the underlying processes of laser-target interaction in a vacuum environment.

It is well-known from mass spectrometric investigations that the amount and ionization degree of the vaporized material depend on the energy deposited into the target. The different regimes of laser ionization, laser desorption, laser vaporization, and laser plasma ionization are characterized by the amounts of deposited energy. The different regimes require different descriptions, because each has its distinctive features determined by a dominating process or several competing processes.

The most common mechanism of laser desorption is a thermally activated process induced by surface heating of the sample (11). In this regime the amount of material transport across the surface is negligible (Figure 1a).

Laser heating of the solid surface and of the induced plume leads to the generation of different chemical species. Ion-molecule reactions are among the favored reaction channels for producing ions which contribute to the variety of important lines in the mass spectra (12). Protonation and alkylation reactions are often the sources of the most characteristic species in the ion cloud (13).

Increasing the energy deposition into the sample the surface temperature reaches a point where material transfer across the surface becomes significant (Figure 1b). In the experiments observable target erosion appears in the form of craters (14). In theoretical terms it means that the energy balance equation has to be supplemented by the balance equations for mass and momentum. The flow, the heating, and the expansion of the evaporated target material are governed by the equations of hydrodynamics (15-17). Solving the coupled partial differential equations of the conservation laws provides

\* To whom correspondence should be addressed. Electronic mail: vertes@ccv.uia.ac.be.

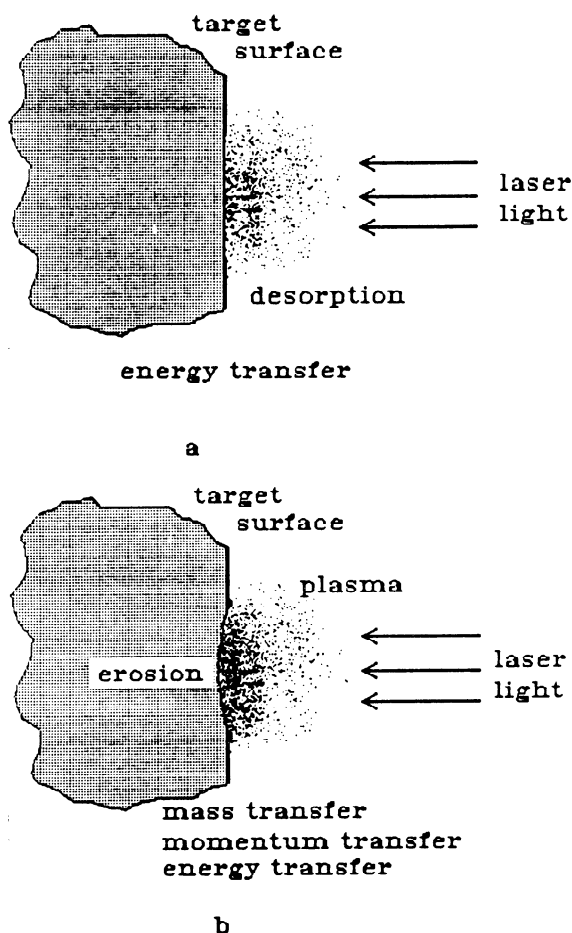


**Figure 1.** Different regimes of laser–target interaction under vacuum. In laser desorption (a) material transport across the surface is negligible. Laser volatilization (b) is characterized by considerable transport of mass, momentum, and energy and occasional plasma formation.

insight into the factors determining crater depth, cloud extension, ion yield, relative sensitivity factors, and ion kinetic energy distributions. Calculated and measured values of these quantities show promising correlations for different lasers and different types of materials (15).

In the present article we exclude the laser desorption regime from the discussion; i.e. we focus our attention to situations where material transport cannot be neglected. Naturally, this is the case in laser sampling experiments and both in mass and optical atomic spectroscopy applications (18).

In order to describe the fate of the laser energy during laser–solid interaction, several processes should be considered. Due to the character of the target, a fraction of the energy is absorbed from the laser pulse while the rest is reflected by the surface. The deposited part of the laser energy is converted into local heat instantaneously, which can in turn diffuse by heat conduction. An increase in temperature may induce appreciable changes in optical and thermal properties of the solid, thus influencing the rate of energy deposition and heat transfer. If the surface temperature is sufficiently high, phase change (melting) may occur and part of the absorbed laser power is expended into the latent heat of transition. Further heating results in the translation of the solid–liquid interface into the bulk, while the surface temperature continues to rise until evaporation commences. Part of the absorbed energy is devoted to the heat of vaporization. Although rapid vapor formation at high temperatures causes significant surface recession, vaporization is not the only and not even the most important crater formation mechanism in many cases. Hydrodynamic effects in which droplets and particulates are expelled from the molten surface layer and ejection

of the melt caused by vapor recoil are among the mechanisms which contribute to the ablation of the target (19, 20).

In the hot vapor excited species, ions and free electrons are generated which interact with the laser light, leading to further heating and ionization. This in turn leads to increased absorption. On the basis of the laser power, this feed-back mechanism may or may not result in a breakdown, i.e. the generation of a fully ionized plasma. In a previous paper we established a criterion for this plasma ignition threshold as a relation of the normal and plasma absorption coefficient (21).

After plasma ignition the laser energy is coupled to the strongly absorbing plume. Plasma temperature can reach extremely high values, and the plume, containing also multiply charged species, becomes luminous. The extremely high energy density of the medium fuels the plasma expansion, and the blow-off material continues its radiation for a long time even after the end of the laser pulse (22).

From the practical point of view, postpulse processes might be just as important. Expansion of the hot cloud of particles continues after laser heating has ceased, and the plume starts to cool down, leading to recombination (23, 24). Atomic emission spectroscopy is based on the line emission emerging from radiative recombination and on other relaxation processes in the postpulse plume (22). Part of the ions detected in a mass spectrometer are also released during the late expansion phase of the plasma.

Vaporization due to Q-switched laser illumination proceeds on the 100-ns time scale. Some laser-induced processes, however, do not cease at this stage. Particulate formation may continue for as long as several hundred microseconds (25–27). Although particulates are very important in the explanation of laser sampling experiments, ion formation, essential in atom and ion sources, is more bound to the vaporization and plasma formation phase.

It is the aim of this paper to assess the importance of different processes taking place in the expanding vapor during and after the laser shot and to compare the temporal behavior of the cloud generated by laser vaporization and by plasma ionization.

## METHODS OF CALCULATION

In order to study pulsed-laser heating and evaporation of solids, we constructed a one-dimensional model consisting of two parts: the first dealt with the heating and melting of the target and predicted the temperature, density, and flow velocity of the particles emerging on the liquid–vapor interface, whereas the second followed the expansion of the plume expelled from the surface. In the following sections we present the framework of the calculations.

**(a) Heating, Melting, and Vapor Formation.** Let us consider a pulsed laser beam impinging perpendicularly on the solid surface. If the beam diameter is much larger than the thermally affected thickness of the solid, the diffusion of the absorbed laser energy can be described by the one-dimensional heat conduction equation with a source term:

$$\frac{\partial T(x,t)}{\partial t} = \frac{\partial}{\partial x} \left[ \left( \frac{K}{c_p \rho} \right) \frac{\partial T(x,t)}{\partial x} \right] + \frac{\alpha}{c_p \rho} I(x,t) \quad (1)$$

where  $T$  denotes the temperature inside the solid,  $x$  is the position measured from the surface,  $t$  is the time, and  $K$ ,  $c_p$ ,  $\alpha$ , and  $\rho$  stand for the thermal conductivity, heat capacity, absorption coefficient, and mass density, respectively.  $I(x,t)$  is the laser irradiance which, assuming a homogeneous absorbing medium, can be written as

$$I(x,t) = I_0(t)(1 - R) \exp(-\alpha x) \quad (2)$$

Here  $I_0(t)$  is the incident laser irradiance and  $R$  is the reflectivity of the surface.

Reliable experimental data on the reflectivity of hot surfaces are rather scarce, although there is strong evidence that in the case of metals the infrared reflectivity drops sharply with increasing temperature whereas the change is less pronounced in the UV domain (19, 20, 28). It is usually assumed that for long wavelengths the temperature dependence of reflectivity can be related to that of the dc conductivity,  $\sigma_0(T)$ , through the following expression:

$$1 - R(T) = [1 - R(T_0)]\sigma_0(T_0)/\sigma_0(T) \quad (3)$$

where  $R(T_0)$  and  $\sigma_0(T_0)$  are the free-electron part of the reflectivity and the dc conductivity of the solid (19).

In order to deal with phase transitions during the heat transfer and to cope with temperature-dependent optical and thermal parameters, eq 1 had to be solved numerically. The finite difference method we employed was similar to the one described by several authors (29–31).

Assuming thermally activated surface vaporization, the flux of atoms crossing the liquid–vapor interface is determined by the actual surface temperature,  $T_s$ , and can be approximated by

$$j(T_s) = Ap(T_s)/\sqrt{2\pi MRT_s} \quad (4)$$

where  $M$  is the molecular mass of atoms,  $R$  is the gas constant, and  $p(T_s)$  is the equilibrium vapor pressure (19). The sticking coefficient,  $A$ , is usually taken to be close to unity in the case of metals. An expression for the temperature dependence of the equilibrium vapor pressure can be obtained by integrating the Clausius–Clapeyron equation:

$$p(T_s) = p_0 \exp(\Delta H_{lv}(T_s - T_{lv})/RTT_{lv}) \quad (5)$$

where  $\Delta H_{lv}$  stands for the heat of vaporization and  $T_{lv}$  is the boiling point at the ambient pressure  $p_0$ . The amount of heat devoted to the vaporization and the thickness of the layer evaporated during the time interval,  $\Delta t$ , are expressed as

$$\Delta Q_{\text{evap}} = j\Delta H_{lv}\Delta t \quad (6)$$

$$\Delta x_{\text{evap}} = \frac{jM\Delta t}{\rho} \quad (7)$$

The initial velocity distribution of particles which come off the surface can be regarded as a half-range Maxwellian; i.e. the velocity component normal to the surface can have non-negative values only (32). The flow velocity of the vapor appearing above the liquid surface can be approximated by the average of the normal velocity component (32):

$$\hat{v}_x = \sqrt{2kT_s/\pi m} \quad (8)$$

where  $k$  is the Boltzmann constant and  $m$  is the mass of an atom.

The main source of positive ions at the onset of vaporization is the thermionic emission from the heated surface, generally described by the so-called Langmuir–Saha equation (28):

$$\frac{n_1}{n_0} \approx \exp\left(-\frac{E_1 - \phi}{kT}\right) \quad (9)$$

where  $n_0$  and  $n_1$  are the number densities of neutrals and singly charged ions, respectively,  $E_1$  is the first ionization potential, and  $\phi$  is the electronic work function.

**(b) Vapor Expansion and Plasma Generation.** As target heating continues and the plume develops with continuously increasing density and temperature, the collisions between particles become frequent enough that the hypotheses of *local thermal equilibrium* for the individual volume elements can be adopted. This means, that, in a sufficiently small region of the plume, thermal equilibrium is established between electrons, ions, and neutrals; that is, they can be characterized with a common temperature and the Saha–Eggert equation

can be utilized for calculating electron, ion, and neutral densities. We consider a quasi-neutral plasma of one chemical element consisting of electrons, atoms, and ions with charge number  $z$ , ranging from  $z = 1$  to  $z = z_{\text{max}}$ . Only thermal ionization due to energetic collisions in the plasma was considered, other processes like charge exchange, excitation, cluster formation, etc. were not included in the model.

Neglecting the possible depression in ionization potentials and the difference between the partition function of ions and neutrals, we can write for each ionization step an appropriate Saha–Eggert equation:

$$\frac{x_e x_z}{x_{z-1}} = \frac{1}{n} \left( \frac{2\pi m_e kT}{h^2} \right)^{3/2} \exp\left(-\frac{E_z}{kT}\right) \quad (10)$$

where  $h$  stands for the Planck constant and  $E_z$  is the ionization energy of the species with a charge number  $z - 1$ . The local number density,  $n$ , is given by  $n = \rho/m$ ;  $\rho$  is the local mass density of the plasma,  $m_e$  is the electron mass, and  $x_z$  and  $x_e$  are defined as  $x_z = n_z/n$  and  $x_e = n_e/n$ .

Supplementing eq 10 with the conservation of matter

$$x_0 + x_1 + x_2 + \dots + x_{z_{\text{max}}} = 1 \quad (11)$$

and with the conservation of charge

$$x_1 + 2x_2 + \dots + z_{\text{max}}x_{z_{\text{max}}} = x_e \quad (12)$$

we obtain a complete set of equations from which the local densities of each component can be obtained. The Newton–Raphson method (33) was used to solve this strongly nonlinear system of equations, ensuring fast and reliable convergence during the iteration.

For the sake of simplicity we neglect the radial thinning of the plume, which is a good approximation if the diameter of the laser focal spot is commensurable or especially if it is much larger than the distance left behind by the plume during the time of investigation. To follow the expansion of the vapor, we then have to solve the one-dimensional equations of hydrodynamics expressing the conservation of mass, momentum, and energy, respectively:

$$\frac{\partial \rho}{\partial t} = -\frac{\partial(\rho v)}{\partial x} \quad (13)$$

$$\frac{\partial(\rho v)}{\partial t} = -\frac{\partial}{\partial x}(p + \rho v^2) \quad (14)$$

$$\frac{\partial}{\partial t} \left[ \rho \left( e + \frac{v^2}{2} \right) \right] = -\frac{\partial}{\partial x} \left[ \rho v \left( e + \frac{p}{\rho} + \frac{v^2}{2} \right) \right] + \alpha \Phi - \epsilon_{\text{rad}} \quad (15)$$

Here  $p$  denotes the local pressure,  $\rho e$  is the local internal energy density,  $\Phi$  is the laser irradiance, and  $\alpha$  and  $\epsilon_{\text{rad}}$  are the linear light absorption coefficient and the radiation power loss emitted in the Bremsstrahlung process, respectively. If the electrons have a Maxwellian distribution of velocities, the total amount of energy emitted per unit volume per unit time is (34)

$$\epsilon_{\text{rad}} = \left( \frac{2\pi kT}{3m_e} \right)^{1/2} \frac{32\pi e^6}{3hm_e c^3} n_e \sum_z z^2 n_z g_z \quad (16)$$

where  $e$  is the electron charge,  $c$  is the velocity of light, and  $g_z$  stands for the Gaunt factor, which is usually close and has been taken equal to unity in our calculations. Assuming that the plasma follows the ideal gas rule, the relation of pressure and internal energy density to the state variables can be written in the form

$$p = (1 + x_e)\rho kT/m \quad (17)$$

$$\rho e = \frac{\rho}{m} \left[ \frac{3}{2}(1 + x_e)kT + \sum_{w=1}^{z_{\text{max}}} (E_w \sum_{z=1}^{z_{\text{max}}} x_z) \right] \quad (18)$$

**Table I. Thermophysical and Optical Parameters of Copper Used in Our Calculations**

	solid	liquid
thermal conductivity, W/(m K)	380	170
specific heat, J/(kg K)	420	494
density, kg/m <sup>3</sup>	8900	7800
mp, K	1356	
$\Delta H_{\text{fusion}}$ , kJ/mol	13.0	
$\Delta H_{\text{lv}}$ , kJ/mol		304.8
reflectivity at 300 K	0.975	
abs coeff, m <sup>-1</sup>	$7.44 \times 10^7$	$7.44 \times 10^7$

where  $E_w$  is the  $w$ th ionization energy.

As it was mentioned earlier, transition between laser vaporization and plasma ignition shows threshold behavior and drastic differences can be observed in characteristic features (e.g. expansion velocities, temperatures, ion energies, etc.) of the plumes generated under the two different regimes. This threshold behavior can be explained by the onset of a feedback mechanism in the absorption of the plume which turns the almost completely transparent vapor into a strongly absorbing, opaque plasma.

Absorption of heated gases that have no molecular absorption bands can be attributed mainly to free-free transitions of electrons in the field of neutrals or ions. Photoionization of excited species may have important contribution only in the case of UV lasers and in the presence of species with low ionization potential (35). Preceding plasma ignition, the plume consisting of largely neutral atoms, interacts with the laser mainly through electron-neutral inverse Bremsstrahlung processes. For this process the absorption coefficient is given by

$$\alpha_{e,n} = [1 + \exp(-h\nu/kT)]Qn_e n_0 \quad (19)$$

where  $\nu$  is the laser frequency,  $T$  is the local plume temperature,  $n_e$  and  $n_0$  are the electron and neutral number densities, and  $Q$  is the cross section of the photon absorption (36). As the vapor temperature and hence the number of charged particles increases, the electron-ion inverse Bremsstrahlung process becomes dominant. The absorption coefficient in this case can be written as follows (34, 36):

$$\alpha_{e,i} = \left[1 - \exp\left(-\frac{h\nu}{kT}\right)\right] \frac{4e^6 n_e}{3hc\nu^3 m_e} \left(\frac{2\pi}{3m_e kT}\right)^{1/2} \sum_z z^2 n_z g_z \quad (20)$$

Equations 5 and 8 completed with the assumption that the vapor temperature at the liquid-gas interface is equal to the actual surface temperature served as boundary conditions for the equations of hydrodynamics. Numerical solution of the problem was based on a finite difference approximation of eqs 13–15 utilizing the scheme of Godunov (37). Details of the algorithm were discussed elsewhere (16).

## RESULTS AND DISCUSSION

Calculations were carried out for the ruby laser-copper interaction at 30 J/cm<sup>2</sup> and at somewhat higher, 36 J/cm<sup>2</sup>, laser energy densities. The temporal intensity profile of the laser pulse,  $I_0(t)$  in eq 1, was approximated by Gaussian distribution of 30-ns full width at half-maximum (see dashed curve in Figure 4). Although the numerical solution of eq 1 enabled the accurate temperature dependence of the thermophysical parameters to be considered, we made distinction only between the solid and the liquid phase, each characterized by one set of thermal parameters, as it is displayed in Table I.

In eq 15 the absorption coefficient,  $\alpha$ , was approximated by the sum of the electron-neutral and electron-ion inverse Bremsstrahlung coefficients given by eqs 19 and 20. Surface

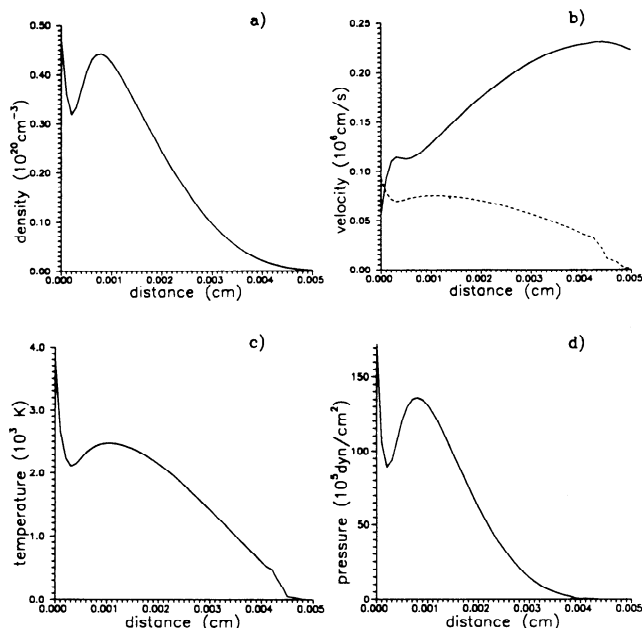


**Figure 2.** Calculated density (a), velocity (b), temperature (c), and pressure (d) profiles at 70 ns. The laser energy fluence was 30 J/cm<sup>2</sup>. The dashed curve in b corresponds to the local sound velocity defined by eq 21.

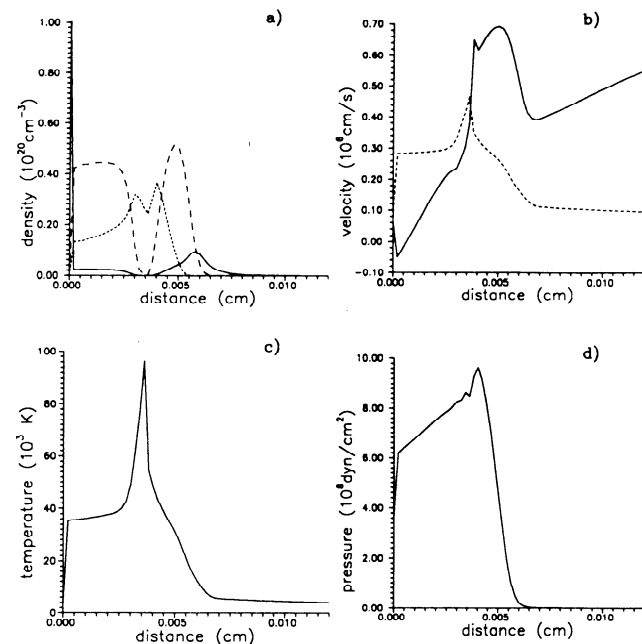


**Figure 3.** Calculated density (a), velocity (b), temperature (c), and pressure (d) profiles at 70 ns. The laser energy fluence was 36 J/cm<sup>2</sup>. The different lines in a correspond to different species: (—) Cu<sup>0</sup>; (---) Cu<sup>+</sup>; (---) Cu<sup>2+</sup>. The broken line in b represents the local sound velocity defined by eq 21.

reflectivity was calculated according to eq 3 on the basis of dc conductivity and on other data (19, 38–40). In the plasma, formation of singly and doubly charged copper ions (ionization potentials  $E_1 = 7.726$  eV and  $E_2 = 20.29$  eV) were investigated.

Results referring to the trailing edge of the laser pulse (70 ns) are presented in Figures 2 and 3, for 30 and 36 J/cm<sup>2</sup> laser fluences. The conspicuous difference in the calculated density, velocity, temperature, and pressure profiles points to the difference in the position of energy deposition.

Below the plasma ignition threshold, the blow-off material remains transparent as long as the laser is on. Therefore the laser can reach the metal surface without appreciable attenuation where a fraction of its energy is absorbed while the rest

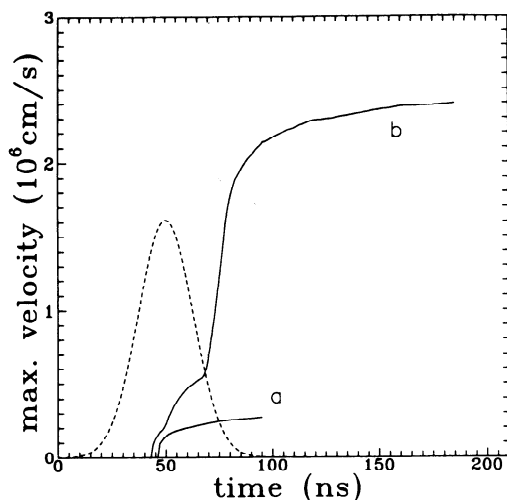


**Figure 4.** Calculated front velocities as a function of time at (a) 30 J/cm<sup>2</sup> and (b) 36 J/cm<sup>2</sup> laser energy densities. The dashed curve represents the temporal distribution of the laser pulse.

is reflected and lost as far as the laser ablation process is concerned. The temperature of the expanding plume never exceeds the surface temperature, and in the vapor thermal ionization is almost completely absent. The plume expands into the vacuum, and its flow becomes supersonic; i.e. the flow velocity exceeds the local velocity of sound, defined as

$$v_s = \sqrt{\gamma kT/m} \quad (21)$$

where  $\gamma = 5/3$  for a gas consisting of atomic species.

In the high-fluence case, the energy delivered to the plume through electron-neutral inverse Bremsstrahlung processes was enough to elevate the temperature close to the surface value, giving rise to high electron density as well as intense light absorption.

In Figure 4 the comparison of maximum flow velocities as a function of time indicates that streaming velocities were almost identical for low- and high-energy fluences until the onset of plasma formation.

In the high-fluence case, at about 50 ns a transition period starts leading to the rapid growth of the plasma, which is apparent from the steep rise in the flow velocity. After breakdown, the incident laser energy is completely deposited into the plasma, increasing its velocity to about  $2.4 \times 10^6$  cm/s, whereas at 30 J/cm<sup>2</sup> the expansion velocity remains about one-eighth of this value due to the lack of direct plume heating. As it is apparent in Figure 3a and c, a highly ionized, hot layer is formed at the plasma front in which the temperature exceeds  $10^5$  K by the end of the laser pulse. These high temperatures result in the production of multiply charged ions. Depending on the local density and temperature the different regions are dominated by different species. Figure 3b and d illustrate the piling up of waves induced by laser heating in the absorption zone and the development of the shock wave driven by the dense, expanding plasma core.

Expansion of the plasma continues after the laser pulse has ceased, and plume properties change considerably during this additional flow. In order to elucidate some of these variations, we traced the expansion further in time.

Figures 5 and 6 show three selected stages of the evolution of density profiles for 30 and 36 J/cm<sup>2</sup> energy fluences, respectively. As time evolves the vapor detaches from the target and a bell-shaped density distribution develops, which drifts towards the vacuum. The motion of the blow-off material can be interpreted as the translation of the center-of-gravity accompanied by the expansion of the cloud.

The fast decay of the density distribution at 30 J/cm<sup>2</sup> and the persistence of a relatively compact core at the higher

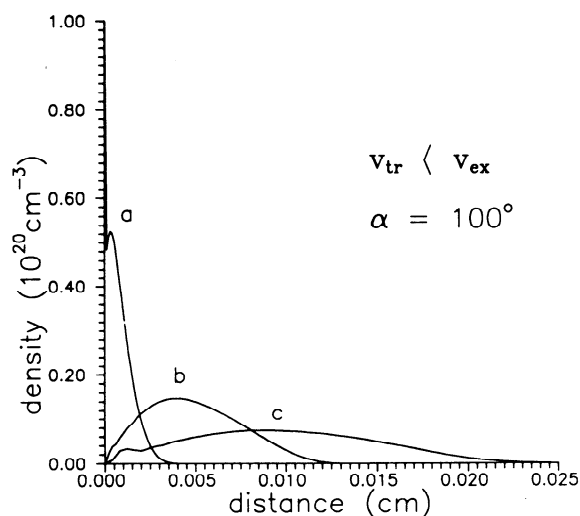


**Figure 5.** Density profiles at (a) 65 ns, (b) 95 ns, and (c) 125 ns. The laser fluence was 30 J/cm<sup>2</sup>. Calculated translation and expansion velocities of the plume were  $v_{tr} = 1.3 \times 10^5$  cm/s and  $v_{ex} = 2 \times 10^5$  cm/s, respectively.

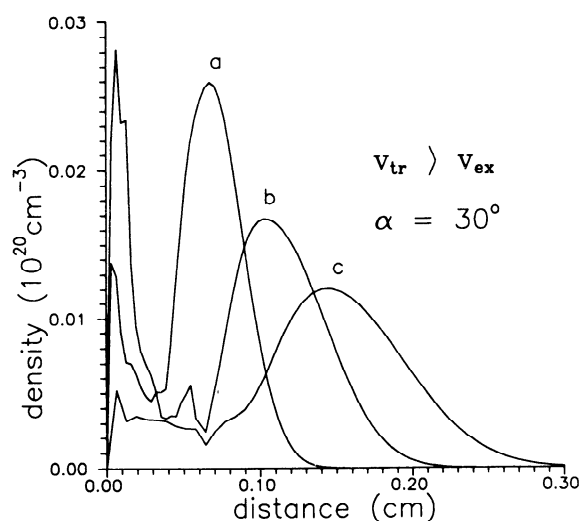


**Figure 6.** Density profiles at (a) 125 ns, (b) 155 ns, and (c) 185 ns. The laser fluence was 36 J/cm<sup>2</sup>. Calculated translation and expansion velocities of the plume were  $v_{tr} = 1.3 \times 10^6$  cm/s and  $v_{ex} = 6.8 \times 10^5$  cm/s, respectively.

energy fluence reflect that the relation between the propagation and expansion velocities is different below and above the plasma ignition threshold. Translation velocities are  $1.3 \times 10^5$  and  $1.3 \times 10^6$  cm/s for the low- and high-fluence cases, respectively. The expansion velocities estimated at the half-maxima of the density distribution curves are  $2 \times 10^5$  and  $6.8 \times 10^5$  cm/s below and above the ignition threshold.

Another feature of the plume formation is that the ratio of propagation and expansion velocities does not change during the postpulse period. It is worth noting that this kind of behavior corresponds to a steadily growing spherical plume in three dimensions drifting along the target normal. The laser blow-off material occupies a conical annular region, and the opening angle is determined by the ratio of the expansion and translation velocities. This observation is justified by laser beam deflection experiments on laser-generated plumes (41). We indicated in Figures 5 and 6 the angle of a hypothetical cone in which a three-dimensional plume would be confined with the same expansion and translation velocities that were obtained in the calculations:  $\alpha = 100^\circ$  for the subthreshold situation, whereas  $\alpha = 30^\circ$  for the plasma ignition case.

Experimental evidence was adduced that laser-generated plasmas exhibit strong forward peaking; moreover, in certain

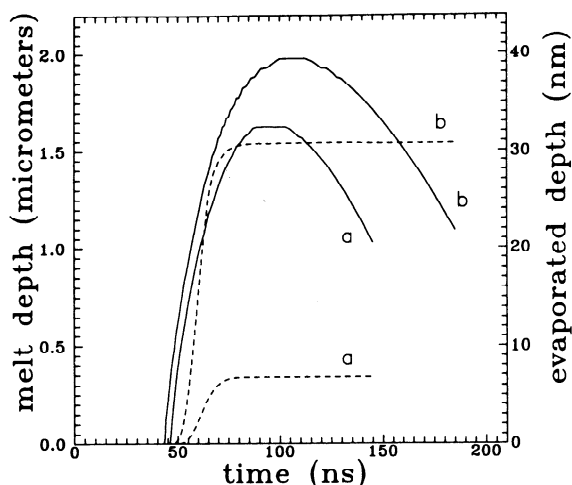


**Figure 7.** Evolution of melt depth (solid curve) and evaporated thickness (dashed curve) with time at (a) 30 J/cm<sup>2</sup> and (b) 36 J/cm<sup>2</sup> laser energy densities.

cases the plume is tightly confined to narrow cylindrical structures (42, 43). In the light of the present calculations this phenomenon could be explained by assuming an essentially planar expansion at the very beginning of the laser–solid interaction accompanied by a significant increase in the velocity component normal to the target surface. Nevertheless, one must not overlook the fact that other factors, e.g. streaming of the vapor out of the crater created by the laser pulse, result also in the decrease of the expansion angle (41).

The agreement between calculated expansion velocities and the results of ion energy measurements is also reasonable. The energy distribution of multiply charged ions stemming from ruby laser–copper interaction were determined by means of a 127° electrostatic analyzer (44). The lowest irradiance limit of these measurements coincided with our 36 J/cm<sup>2</sup> calculation. In these experiments only two ionic species, Cu<sup>+</sup> and Cu<sup>2+</sup>, were identified. The center of the measured energy distribution for Cu<sup>2+</sup> ions was at 250 eV corresponding to  $2.8 \times 10^6$  cm/s ion velocity, which is in good agreement with the calculated  $2.4 \times 10^6$  cm/s terminal plasma front velocity.

Despite the promising correlation we would like to emphasize that this kind of comparison is always subject to ambiguity. Apart from the significant uncertainties in laser power density determinations, our model was designed to describe planar expansion which was obviously not the case in the aforementioned experiment. On the other hand we did not address the question how velocity distributions of different species change when the assumption of local thermal equilibrium ceases to hold. Furthermore we did not consider the effect of the external field penetration to the low-density regions of the plasma. Nevertheless, it is reasonable to assume that the terminal front velocity represents the mean velocity of ions even after the transition to collision-free flight.

Finally, we consider the problem of crater formation. The evolution of the melt depth with time along with the corresponding evaporated thickness is presented in Figure 7 for both laser fluences. One can observe that the melt front penetrates rapidly into the solid and, after having reached the maximum depth (1.63 μm for 30 J/cm<sup>2</sup> and 1.98 μm for 36 J/cm<sup>2</sup>), it recedes back due to the resolidification with a somewhat lower velocity. Through the comparison of melt front histories with the shape of the laser pulse (see Figure 4), it is apparent that melting continues even after the incident laser pulse has been extinguished and a region thicker than 1 μm remains molten for almost 100 ns in both cases. In our model material removal is solely attributed to vaporization and, therefore, the thickness of the evaporated layer can be regarded as a lower bound to the crater depth. Subthreshold

behavior resulted in low evaporated thickness, whereas in the higher fluence case the amount of material removed by evaporation was increased significantly due to the exponential dependence of evaporation rate on the surface temperature.

As it was discussed above, in pulsed-laser ablation experiments, the splashing of the melt due to vapor recoil is observed. If we assume that the melt is completely ejected before resolidification, the maximum and the melt depth curve serves as an upper limit for the measured value. This assumption is supported by measurements on copper where a 2.2 μm deep crater was produced by a 44 J/cm<sup>2</sup> irradiance Q-switched ruby laser pulse (28). Extrapolating our calculated maximum melt front position to this fluence, we obtain 2.6 μm, a fair estimate for the measured crater depth.

## CONCLUSIONS

The diversity of phenomena occurring during laser ablation and the lack of reliable experimental data on the high-temperature behavior of solids compelled us not to make any pretense of describing laser–solid interaction in detail. We rather tried to find a simple model to account for pulse melting and vaporization of metals as well as for the absorption and ignition of the plume. The fair agreement between the calculated and measured ion velocities and the feasible upper and lower limits for the crater depth, as well as the prediction of the plume propagation confined in a conical spatial region, indicate that laser vaporization and plasma ionization can be treated in the framework of the presented model.

Nevertheless, the general formulation of the problem makes it difficult to account for all the events of practical and theoretical interest during the laser–solid interaction. The applicability of the model at high irradiances could be stretched by taking into account more ionization steps, employing a more realistic equation of state, and possibly considering critical phenomena.

## LITERATURE CITED

- (1) Conzemius, R. J.; Capellen, J. M. *Int. J. Mass Spectrom. Ion Phys.* **1980**, *34*, 197.
- (2) Vertes, A.; Gijbels, R.; Adams, F. *Mass Spectrom. Rev.* **1990**, *9*, 71.
- (3) Jansen, J. A. J.; Witmer, A. W. *Spectrochim. Acta* **1982**, *37B*, 483.
- (4) Kagawa, K.; Matsuda, Y.; Yokoi, S.; Nakajima, S. *J. Anal. At. Spectrom.* **1986**, *3*, 415.
- (5) Broekaert, J. A. C.; Leis, F.; Raeymaekers, B.; Zaray, Gy. *Spectrochim. Acta* **1988**, *43B*, 339.
- (6) Gray, A. L. *Analyst* **1985**, *110*, 551.
- (7) Arrowsmith, P. *Anal. Chem.* **1987**, *59*, 1437.
- (8) Adams, F.; Vertes, A. *Fresenius' J. Anal. Chem.* **1990**, *337*, 638.
- (9) Zhu, J.; Yeung, E. S. *Anal. Chem.* **1989**, *61*, 1906.
- (10) Li, L.; Lubman, D. M. *Anal. Chem.* **1989**, *61*, 1911.
- (11) Vertes, A.; Juhasz, P.; Balazs, L.; Gijbels, R. *Microbeam Anal.* **1989**, *1989*, 273.
- (12) Visvanadham, S. K.; Hercules, D. M.; Schreiber, E. M.; Weller, R. R.; Giam, C. S. *Anal. Chem.* **1988**, *60*, 2346.
- (13) Vertes, A.; Juhasz, P.; Gijbels, R. *Fresenius' Z. Anal. Chem.* **1989**, *334*, 682.
- (14) Chen, G.; Yeung, E. S. *Anal. Chem.* **1988**, *60*, 864.
- (15) Vertes, A.; Juhasz, P.; De Wolf, M.; Gijbels, R. *Int. J. Mass Spectrom. Ion. Processes* **1989**, *94*, 63.
- (16) Vertes, A.; Juhasz, P.; De Wolf, M.; Gijbels, R. *Scanning Microsc.* **1988**, *2*, 1853.
- (17) Vertes, A.; Juhasz, P.; De Wolf, M.; Gijbels, R. *Adv. Mass Spectrom.* **1989**, *11*, 1638.
- (18) Koppenaal, D. W. *Anal. Chem.* **1988**, *60*, 113R.
- (19) von Allmen, M. *Laser-Beam Interactions with Materials*; Springer: Berlin, 1987; Chapters 2 and 5.
- (20) Kelly, R.; Rothenberg, J. E. *Nucl. Instrum. and Methods Phys. Res.* **1985**, *B7/8*, 755.
- (21) Vertes, A.; De Wolf, M.; Juhasz, P.; Gijbels, R. *Anal. Chem.* **1989**, *61*, 1029.
- (22) Kim, Y. W. *Fundamentals of Analysis of Solids by Laser-Produced Plasmas*. In *Laser-Induced Plasmas and Applications*; Radziemski, L. J., Cremers, D. A., Eds.; Marcel Dekker, Inc.: New York, 1989; pp 327–346.
- (23) Pitsch, P.; Rohr, K.; Weber, H. *J. Phys. D* **1981**, *14*, L51.
- (24) Afanas'ev, Yu. V.; Rozanov, V. B. *Sov. Phys.—JETP (Engl. Transl.)* **1972**, *35*, 133.
- (25) Huie, C. W.; Yeung, E. S. *Appl. Spectrosc.* **1986**, *6*, 863.
- (26) Huie, C. W.; Yeung, E. S. *Anal. Chem.* **1986**, *58*, 1989.
- (27) Kimbrell, S. M.; Yeung, E. S. *Spectrochim. Acta* **1986**, *43B*, 529.
- (28) Ready, J. F. *Effects of High Power Laser Radiation*; Academic: New York, 1972; Chapters 3 and 4.

- (29) Baeri, P.; Campisano, S. U.; Foti, G.; Rimini, E. *J. Appl. Phys.* **1979**, *50*, 788.
- (30) Wood, R. F.; Giles, G. E. *Phys. Rev. B* **1981**, *23*, 2923.
- (31) Jain, A. K.; Kulkarni, V. N.; Sood, D. K. *Appl. Phys.* **1981**, *25*, 127.
- (32) Kelly, R. J. *Chem. Phys.* **1990**, *92*, 5047.
- (33) See for example: *Numerical Analysis*; Burden, R. L., Faires, J. D.; Reynolds, A. C., Eds.; Prindle, Weber & Schmidt: Boston, 1978; pp 443-450.
- (34) Spletzer, L. *Physics of Fully Ionized Gases*; Interscience Publishers: London, 1956; pp 147-149.
- (35) Rosen, D. I.; Hastings, D. E.; Weyl, G. M. *J. Appl. Phys.* **1982**, *53*, 5882.
- (36) Root, R. G. Modelling of Post-Breakdown Phenomena. In *Laser-Induced Plasmas and Applications*; Radziemski, L. J., Cremers, D. A., Eds.; Marcel Dekker, Inc.: New York, 1989; pp 69-103.
- (37) Godunov, S. K.; Zabrodin, A. V.; Prokopov, G. P. *USSR Comput. Math. Math. Phys. (Engl. Transl.)* **1961**, *6*, 1020.
- (38) *Handbook of Optical Constants of Solids*; Palik, E. D., Ed.; Academic: Orlando, F 1985; pp 280-286.
- (39) *Tables of Physical and Chemical Constants*; Kaye, G. W. C., Laby, T. H., Eds.; Longman: London, 1973; p 102.
- (40) *American Institute of Physics Handbook*, 3rd ed.; McGraw-Hill: New York, 1972; Section 4.
- (41) Chen, G.; Yeung, E. S. *Anal. Chem.* **1988**, *60*, 864.
- (42) Irons, F. E.; McWhirter, R. W. P.; Peacock, N. J. *J. Phys. B* **1972**, *5*, 1975.
- (43) Doschek, G. A.; Feldman, U.; Burkhalter, P. G.; Finn, T.; Feibelman, W. A. *J. Phys. B* **1977**, *10*, 1977.
- (44) Goto, T.; Kishi, K.; Okuda, T. *Kaku Yugo Kenkyu* **1982**, *47*, 592.

RECEIVED for review July 20, 1990. Accepted October 29, 1990.  
 This work was partly supported by the Belgian Nationaal Fonds voor Wetenschappelijk Onderzoek (Belgian National Science Foundation). L.B. is indebted to The Soros Foundation—Hungary for financial support. This publication forms part of research results in a project initiated by the Belgian State—Prime Minister's Office—Science Policy Programming.